Glass Europe Vol. 3 (2025) 221-237
https://doi.org/10.52825/glass-europe.v3i.2865

Submitted: 15 Jul. 2025 | Accepted: 02 Oct. 2025 | Published: 24 Nov. 2025

Thermal Poling Assisted Ion Exchange in LAS Glass and Glass-Ceramic

Jonas Hildebrand[1] and Christian Roos[1]

[1]Institute of Mineral Engineering, RWTH Aachen University, Aachen, Germany

Abstract. An open electrode thermal poling setup was used to introduce Na^+ and K^+ cations from chloride salt coatings into the surface of LAS glass. The thermal poling was performed at 200 °C for 180 min and 540 min at poling currents of 50 µA and 200 µA. Na^+ and K^+ migrate from the salt coatings along the electric field lines into the glass surfaces up to 14 µm and 4 µm in depth, respectively. As these cations are larger than the contained Li^+-ions, the induced stresses lead to an increase of surface hardness by ca. 15 % in the ion exchanged areas. Etching trials with 5 % HF solution revealed a faster etching of these Na^+ and K^+ enriched surface areas. The ceramisation of the treated samples led to uneven surfaces presumably due to the influence of Na^+ and K^+ on local viscosity in combination with altered crystallisation behaviour. The introduced cations accumulate in the valleys of the surface topology in a 1-2 µm thin glassy surface layer. Contrary to the glass samples, these areas etch away more slowly in the etching trials and reveal protruded domains where the salt crystal contact areas (abbreviated as cca) were in first place. The high quartz solid solution crystal content in the surface is highest for NaCl coated samples followed by KCl coated samples and uncoated but thermally poled samples.

Keywords: Thermal Poling, Ion Exchange, Glass-Ceramics

1. Introduction

The method of thermal poling traces back to the 1960s when the phenomenon of “electrode polarisation” occurred in glasses when exposed to a strong electric field. [1], [2], [3] At elevated temperatures, where glasses show ionic conductivity, a directed movement of network modifier ions in the glass can be observed. The respective cations move away from the positively charged anode towards the negatively charged cathode. Over time a depletion of these network modifier ions develops at the anode faced glass surface leaving behind negative charges (non-bridging oxygens, NBOs) which result in the build-up of a space charge opposite to the external electric field. With the growth of this depletion layer, the space charge will also grow and eventually cancel out the outer electric field and therefore end the thermal poling process. During this thermal poling treatment different charge compensating processes take place in the depletion layer, e.g. the combination of NBOs to BOs, resulting in an irreversible changed glass structure. [4], [5] In general, thermal poling leads to a polymerisation of the glass structure, which in turn leads to different property changes in a surface layer just a few micrometres thick compared to the original glass.

Thermal poling can alter the material properties in many ways. For example, it can cause nonlinear optic behaviour in glasses like the second harmonic generation or change the refractive index of the glass surface. [6], [7], [8], [9], [10] Also, mechanical advantage can be drawn from these treatments, as the hardness and wear resistance can be increased. [11], [12] Moreover, thermal poling can be used to manipulate metal nanoparticles embedded in the

glass structure. [13], [14] Another widely used application of a thermal poling setup is the anodic bonding of silicon to silicate glass (e.g. Pyrex) for example for the production of pressure sensors and accelerometers. [15]

The use of an electric field to accelerate the conventional ion exchange process during chemical strengthening of glasses is not a new approach. Different studies have shown the benefits of adding electrodes to the salt bath and glass sheets to drive K^+ ions towards and into SLS glasses. [16], [17], [18], [19] Even modifications of the conventional salt bath setup have been made by transferring the liquid salts into plastic pastes to form a simplified, layered ion exchange setup of electrode-paste-glass. [20] However, all these approaches come from the idea of using nitrate salt melts at quite high temperatures (~ 400 °C). In this work the motivation was to use a given thermal poling setup with open electrode configuration and use the electric field as a driving force to insert Na^+ or K^+ ions from solid chloride salts into the anode side surface of Lithium-Aluminosilicate glass at much lower temperatures around 200 °C.

2. Experimental

An open electrode setup for the thermal poling treatments was used in which the glass samples are placed on a bottom sheet electrode with the top electrode consisting of a thin platinum wire floating three millimetres above the sample surface (see Figure **1**). A detailed description of the setup can be found elsewhere. [21] The open configuration allows different coatings of the sample to be tested without interfering with the top electrode material.

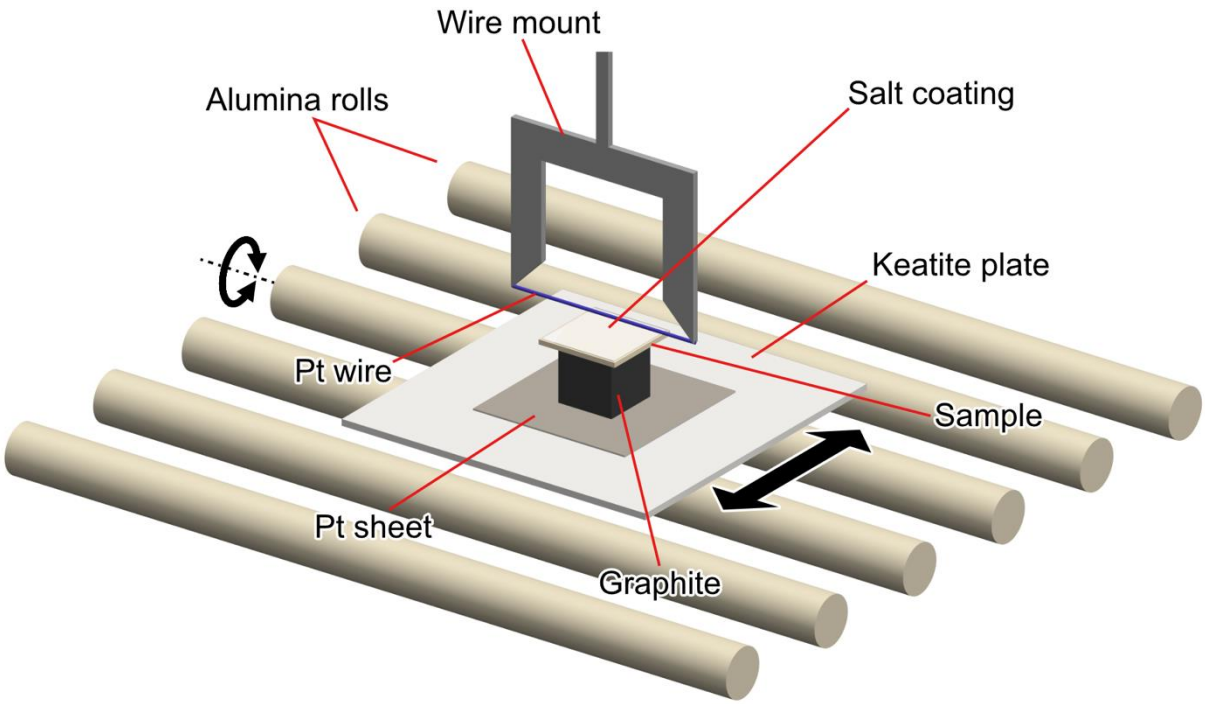

***Figure 1**. Sketch of the used thermal poling setup.*

The glass used for a thermal poling assisted ion exchange process was a LAS glass, for composition see Table **1**. From a 200 mm x 200 mm glass sheet, samples with dimensions of 25 mm x 50 mm were cut and afterwards ground and polished from both sides and etched in a 1:1 mixture of H_2SO_4 and HF for three minutes to achieve a smooth surface finish.

***Table 1**. Composition of the used LAS glass analysed using X-ray fluorescence spectroscopy (XRF) and inductively coupled plasma optical emission spectrometry (ICP-OES).*

Oxide	Mass fraction in %	Oxide	Mass fraction in %
SiO_2	66.73	ZrO_2	1.20
Al_2O_3	19.22	As_2O_3	0.99
Li_2O	3.77	BaO	0.84
TiO_2	2.72	HfO_2	0.32
MgO	2.05	K_2O	0.26
ZnO	1.85	Na_2O	0.13

The glass samples were coated from one side with either NaCl or KCl by first preparing saturated aqueous solutions for both salts. This was done by adding the salts to deionised water until insoluble sediments of the salts remained at the bottom of the test tubes. Because of the bad wetting behaviour of these solutions on the glass surfaces a spin coating process with an external heat source was used. For this, a 3D-printed mount to centre and hold the samples was attached to a small electric engine. With a variable voltage supply the spin rate of the sample could be controlled to be sufficient for a complete spreading of the salt solutions. The process was performed in three steps. First, the sample was heated to over 100 °C with a heat gun. Then the aqueous salt solution was given onto the spinning sample's surface using a small pipette. Afterward, the heat gun and spinning were maintained until all water evaporated. The resulting salt coatings consisted of individual small salt crystals, distributed randomly over the glass surfaces (see Figure **2** a)).

The reverse side of each sample was coated with "PLANOCARBON" graphite by Plano GmbH to assure a good electrical conductivity to the bottom electrode. This graphite paste was applied with a small brush and after drying for about one hour the solid graphite layer was ground plane with 600 grid sandpaper.

For both salt coatings, a set of four thermal poling parameters was chosen, see Table **2**. In addition, a coated sample of each set was exposed to the poling temperature of 200 °C without an electric field to serve as a reference.

***Table 2**. Thermal Poling parameters and corresponding sample numbers.*

	NaCl		KCl	
	180 min	540 min	180 min	540 min
0 µA	-	09	-	10
50 µA	01	03	05	07
200 µA	02	04	06	08

Every sample was poled in duplicates simultaneously, so that one half of the samples could remain glassy (referring to as sample set a), whereas the other half was ceramised after the thermal poling (referring to as sample set b). After the poling, the salt coatings were removed by first rinsing with tap water, afterwards with deionised water and finally cleaning the whole sample with acetone. Sample set b was ceramised by heating to 860 °C with a ramp of 10 $K \cdot min^{-1}$ and after a 10-minute dwell, letting the furnace cool down to room temperature. All thermal poling and ceramisation heat treatments were performed in a specifically built ceramisation furnace by Thermo-Star GmbH.

The surface textures were analysed using a laser scanning Microscope VK-X3000 with integrated white light interferometer by KEYENCE. EDX measurements and SEM imaging were performed on a Zeiss GeminiSEM with 1 kV acceleration voltage for microstructure imaging and 15 kV for EDX measurements, looking both on top of the anode side surfaces and

on cross sections. Prior to the investigation the samples were polished up to 0.6 µm with diamond suspension and using a vibration polishing machine QPOL VIBRO by ATM Qness GmbH.

Nanoindentation of sample set a was done on an Anton Paar NHT^3 nanoindenter with a diamond indenter tip of Berkovich geometry. For all measurements a maximum load of 100 mN was set with a loading and unloading time of 30 seconds.

The XRD measurements of sample set b were performed on an Empyrean 3rd Gen. from Malvern PANalytical using a chromium x-ray tube with $\lambda_{Cr,K\alpha}$ = 2.28976 Å, U = 30 kV and I = 50 mA. Measurements of the anode side surfaces were made under 10 different incident angles ranging from 0.4° to 20° to increase the information depth with each step. High quartz solid solution (HQSS) content was calculated with the K-factor method using an external SiO_2 standard. The standard was measured at the beginning and at the end of the whole measuring procedure to compensate for ageing of the x-ray tube.

The etching trials on the anode side surface were done using 5 % HF. On each sample two circular etching areas with a diameter of 17 mm were bordered by pressing rubber rings on the glass surface and therefore creating a sealed cylindrical mould for the etching solution. 500 µl of HF were given in each mould and removed after 15 minutes. The depth of the etching edges as well as the etched surface areas were inspected via white light interferometry (WLI).

3. Results and Discussion

3.1. Surface Textures

After the thermal poling treatments, on a few samples a change in reflectivity of the treated anode side surface was visible with the naked eye. Therefore, all samples were inspected optically under a microscope with an integrated white light interferometer (WLI). For samples 04a, 06a, 07a and 08a rectangular areas, ranging in size from 50 µm to over 200 µm, appeared. These areas protrude from the surrounding surface about 50 nm, see Figure **2** b). The size comparison with the salt coated samples before thermal poling treatments (Figure **2** a)) implies, that these regions are the contact areas of the salt crystals to the glass surface and therefore the areas where Na^+ and K^+ ions entered the glass. This assumption is verified in the next chapter.

The measurable protrusion of these salt crystal contact areas (abbreviated as cca) is most likely due to the volume increase accompanied by the incorporation of larger Na^+ or K^+ ions into the glass network, compared to the Li^+ ions which were there in first place.

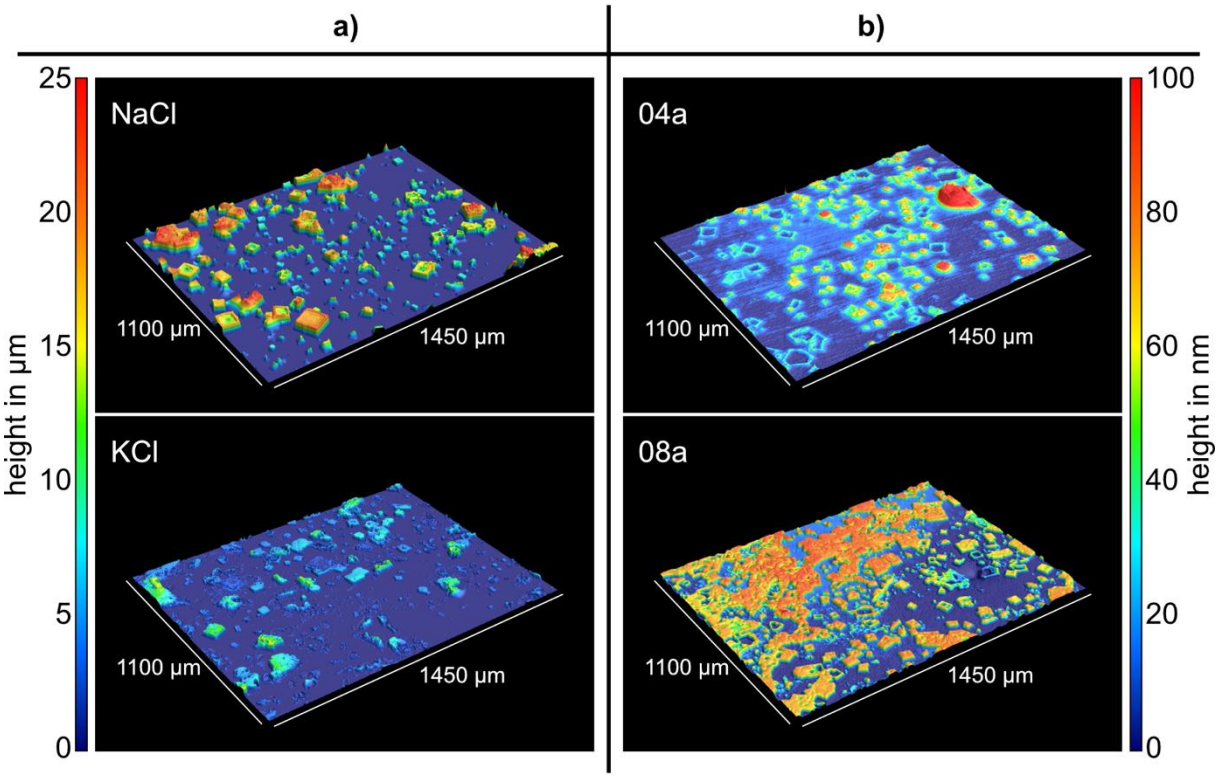

***Figure 2**. Topologies of a) salt coatings before thermal poling and b) sample surfaces after thermal poling treatments and cleaning off the salt coatings. For better visibility the z-axes are magnified by a) 200 % and b) 20000 %. The salt crystal sizes before thermal poling coincide with the protrusion areas afterwards.*

For sample set b, i. e. after ceramisation, the glass samples show uneven and rough surfaces (Figure **3**). With stronger thermal poling (higher poling current and longer poling time) the surface roughness increases as shown in Table **3**. The arithmetical mean height S_a ranges from just a few nanometres to over 1.4 µm.

***Table 3**. Surface roughness values for all thermally poled and ceramised samples.*

Sample	01b	02b	03b	04b	05b	06b	07b	08b	09b	10b
S_a in µm	0,006	0,767	0,156	1,241	0,005	0,195	0,161	1,474	0,018	0,003

The WLI images show that most visible crystal contact areas on sample set b are in the valleys of the surface topology. This suggests a different crystallisation process in the Na^+ and K^+ enriched areas as the reason of the rough surface. Assuming an earlier start of crystallisation or an eventually higher crystal content in these areas combined with the relatively low viscosity at the crystallisation temperature of 860 °C, the surface roughness could be the result of piled up material between the salt crystal contact areas. As the crystallisation of HQSS is associated with a volume change, it could provide a driving force for the piling up of remaining glass phase in between. To make sure that the observed surface roughness is a result of the crystallisation, two additional samples with the same treatment parameters (coating, poling time, poling current) as samples 04 and 08 were prepared and heated to 800 °C after poling treatments. The temperature was chosen to just barely avoid crystallisation but to lower the viscosity of the glass. With that it was possible to see, whether potential compression stresses in the crystal contact areas unload before crystallisation and could lead to the surface roughness. After this additional heat treatment, all samples showed the surface topologies as in

Figure **2**, which means that the unevenness of the glass-ceramics develops only during crystallisation.

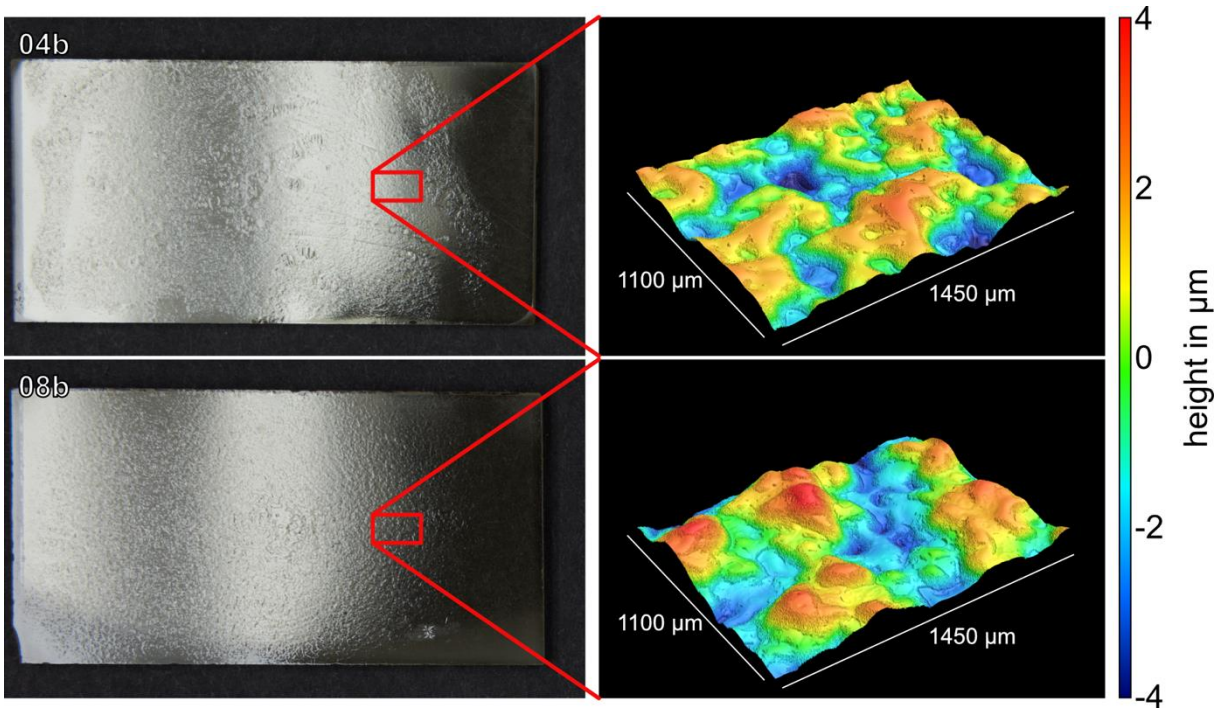

***Figure 3**. Sample surfaces after ceramisation. For better visibility the z-axes are magnified by 2000 %.*

3.2. SEM and EDX

SEM imaging and EDX measurements of the anode side surfaces and of cross sections were conducted to quantify the Na^+ and K^+ penetration into the glass. EDX mappings of the previously WLI-analysed salt crystal contact areas are shown in Figure ***4***. Na^+ and K^+ are enriched in these areas, which actually confirms the aforementioned assumption that these are the contact areas of salt crystals and glass surface. EDX measurements of the cross sections (see Figure ***4***) have been performed showing that firstly, Na^+ and K^+ diffuse perpendicular to the surface to greater depths with minimal lateral diffusion leading to clearly delimited areas of high Na^+ and K^+ concentration, respectively. Secondly, the penetration depth depends on the species, as Na^+ reaches up to 14 µm into the glass surface whereas the concentration profile of K^+ ends at around 4 µm. The first observation can be explained by the electric field of the thermal poling process which is applied across the glass sample and acts as a driving force for the ion movement. This shows that the alkali ions only move along the electric field lines through the glass network with minimal lateral diffusion. The different penetration depths of Na^+ and K^+ are a result of the different diffusivities. It has been shown in different studies that Na^+ is more mobile in a silicate glass network because of its smaller ion radius and the activation energy and frequency of diffusion. [22], [23], [24] Bearing this in mind, it is self-explaining that the diffusion depth of Na^+ is considerably larger than for K^+ given the same poling current and time.

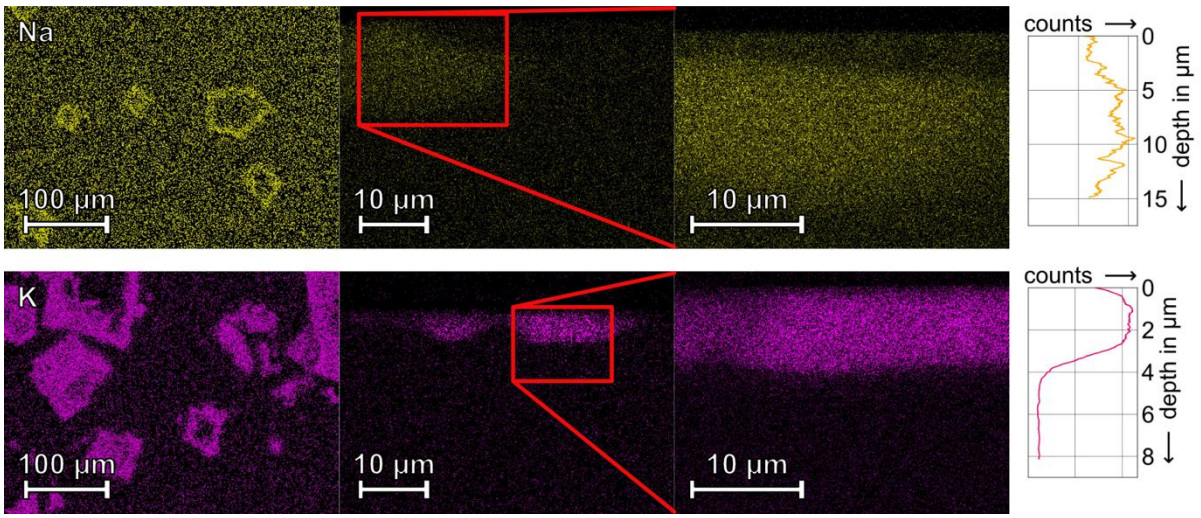

***Figure 4**. EDX measurements of samples 04a (top) and 08a (bottom). On the left are element mappings from the top view of the anode side sample surface, the right images are cross-sectional mappings. On the right are results from line scans made perpendicular to the sample surface in the cross-sections.*

Additionally, the effective diffusion coefficients D_{Na} and D_K can be calculated from the obtained EDX-data. For all eight thermally poled samples EDX line scans were taken (see Figure **5**) so that for each sample D_{Na} and D_K can be calculated using following equation (mean squared displacement or Einstein-Smoluchowski-relation [25]):

$$\boldsymbol{D = \frac{\tau^2}{2t}} \tag{1}$$

In this equation τ is the penetration depth of either Na^+ or K^+ and t is the treatment time. The calculated diffusion coefficients are presented in Table **4**.

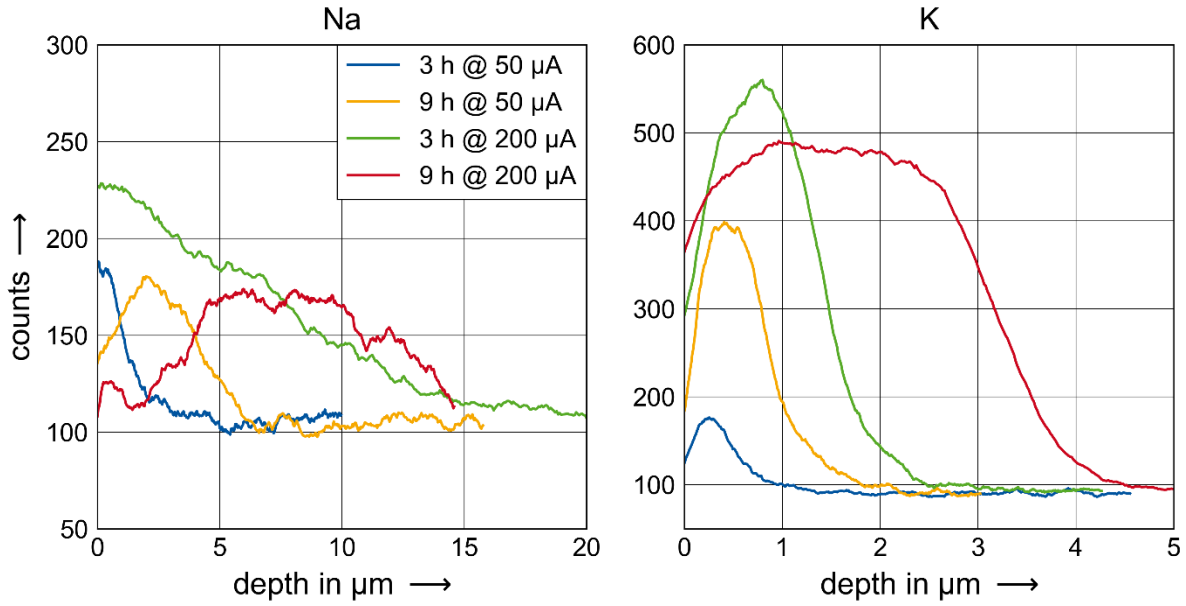

***Figure 5**. Na and K progressions over depth from EDX line scans for all thermally poled samples.*

For Na the diffusion coefficients range from about 10^{-15} m^2/s to 10-16 m^2/s, for K the values are a magnitude smaller, ranging from 10^{-16} m^2/s to 10^{-17} m^2/s. In literature values from D_{Na} = 10^{-15} m^2/s [26], [27] to 10^{-17} m^2/s [23], [28] and D_K = 10^{-17} m^2/s [23] to 10^{-19} m^2/s [29] can

be found for different glass compositions (B_2O_3-Al_2O_3-SiO_2 [26], Na_2O-Al_2O_3-SiO_2 [27], Rhyolithe [23], SiO_2 [28], Na_2O-CaO-SiO_2 [29]). This shows a slightly faster diffusion in this study which is most likely due to the external electric field that drives the directed diffusion. However, it needs to be kept in mind that firstly the literature values given here are for different glass compositions as no values could be found for LAS-glasses, and secondly that the measurements in this study were only performed at a single site on each sample. This means that the values in Table **4** are only a rough estimation and should not be treated as anything more than that.

***Table 4**. Calculated diffusion coefficients for Na and K from measured penetration depths.*

D in m^2/s	Na		K	
	180 min	540 min	180 min	540 min
50 µA	$4{,}2 \cdot 10^{-16}$	$5{,}6 \cdot 10^{-16}$	$4{,}6 \cdot 10^{-17}$	$6{,}2 \cdot 10^{-17}$
200 µA	$1{,}2 \cdot 10^{-14}$	$3{,}5 \cdot 10^{-15}$	$2{,}9 \cdot 10^{-16}$	$3{,}1 \cdot 10^{-16}$

After ceramisation which includes heating to 860 °C the accumulation of externally introduced alkali ions at the anode side surface nearly disappears for Na^+ and weakens for K^+, see Figure **6**. This is a result of diffusion at a temperature of 860 °C needed for the crystallisation of the main crystal phase, HQSS. [30] The much faster diffusion of Na^+ helps by evening out the concentration profile so that after ceramisation it vanishes completely. The K^+ ions on the other hand are larger and therefore slower in diffusion. In combination, the concentration profile does not smoothen that fast and the forming crystals lead to a segregation. The EDX mappings in combination with SEM imaging (see Figure **6**) show, that the K^+ accumulation in sample GC08-08b is mainly present in the 1-2 µm thin glassy surface layer.

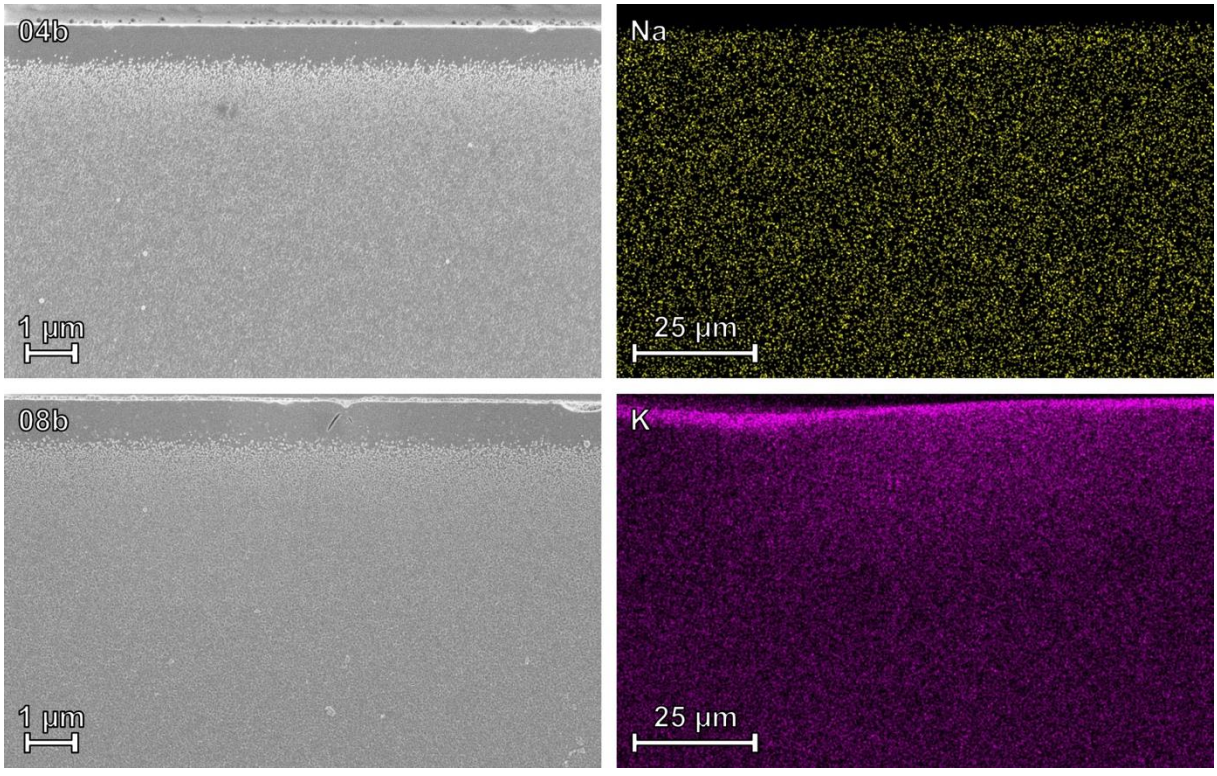

***Figure 6**. Cross-sections of samples 04b (top) and 08b (bottom). On the left SEM imaging of the microstructure can be seen, on the right the according element mappings by EDX measurements.*

EDX mappings from the anode side surface reveal slight deviations in concentrations of Na^+ and K^+ for samples 04b and 08b, respectively (Figure **7**). For the NaCl coated sample 04b no crystal contact areas are visible anymore but the KCl coated sample 08b still shows K^+ enriched areas in accordance with the contact areas on the glass surface seen in Figure ***4***. For both coating types, the Na^+ and K^+ enrichment is present in the valleys of the surface topology which adds to the surface roughness formation mechanism mentioned in the previous chapter.

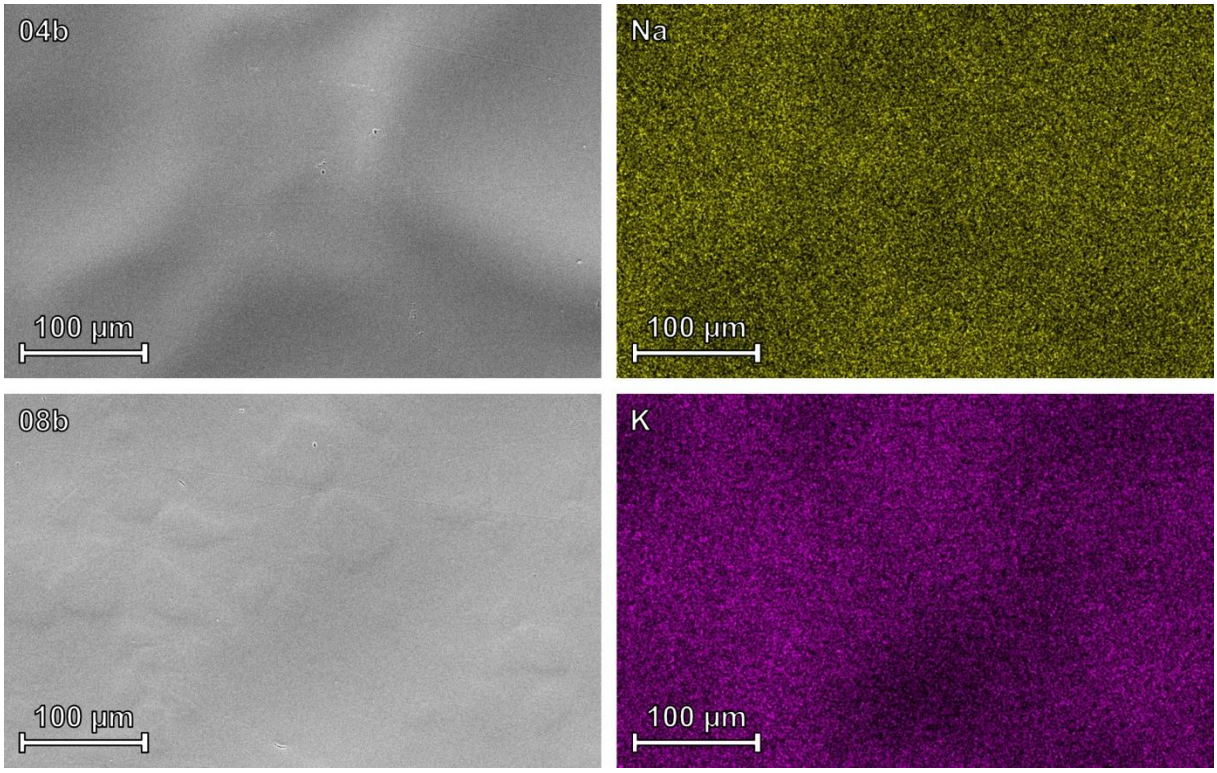

Figure 7*. SEM imaging and element mappings of anode side surfaces of samples 04b (top) and 08b (bottom).*

3.3. Nanoindentation

Hardness testing was done for all samples where crystal contact areas were visible and measurable after thermal poling treatments in the glassy state (sample set a), i. e. where the poling parameters were sufficient to introduce a high amount of Na^+ and K^+ into the glass surface. This means no data is present for samples 01a, 02a, 03a and 05a. Five indents were placed on the crystal contact areas and five in between for each of the other samples, see exemplary microscopy images of samples 04a and 08a in Figure **8**.

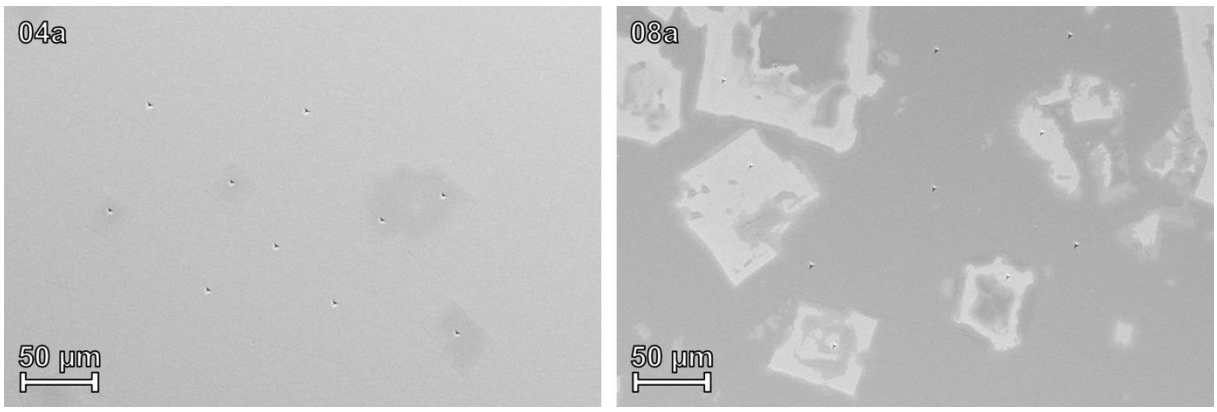

***Figure 8**. SEM images of indent placements on 04a and 08a. The Na^+ and K^+ enriched areas are visible due to the slight mass contrast to the surrounding glass.*

The results of these tests are shown in Figure **9**. For each salt coated and poled sample the hardness of the alkali enriched crystal contact areas is higher (ca. 8.2 GPa) compared to the uncoated areas beside (ca. 7 GPa). The highest hardness was measured on the crystal contact areas of sample 08a with 8.7 GPa. The coated reference samples 09a and 10a as well as a solely polished green glass show hardness values of 8 GPa. An uncoated but thermally poled (200 µA for 9 h) glass sample shows a hardness of 7 GPa, the same as the uncoated areas of the otherwise coated samples. Two main findings can be determined from this: firstly, the surface hardness increases by introducing Na^+ or K^+ into the glass via thermal poling and secondly, the surface hardness overall decreases due to thermal poling treatments.

The first point is a direct result of compressive stresses due to the introduction of large Na^+ or K^+ ions into the glass network. Moreover, as K^+ is larger than Na^+ the compressive stress introduced and therefore the hardness should be higher for the KCl coated samples, at least for the same poling parameters. This is true for samples 04a and 08a but as there is no data for the other three pairs of same poling parameters this point cannot be clarified conclusively.

The hardness decrease due to thermal poling is counterintuitive to the general thermal poling effects on glass structure. As several studies have shown ([5], [11], [12]) the degree of polymerisation in the depletion layers of thermally poled glasses increases due to NBO recombination to BOs and eventually leads to a rise in hardness of this layer. But this is only valid for blocking thermal poling conditions. Other studies with open electrode setups and controlled poling atmospheres ([11], [31], [32]) have found that water in the atmosphere acts as a charge compensation in the depletion layer and forms Si-OH groups with NBOs, suppressing a polymerisation of the glass network. This leads to an opposite effect regarding the surface hardness and therefore explains the decrease of hardness in this study as the used setup here is an open one.

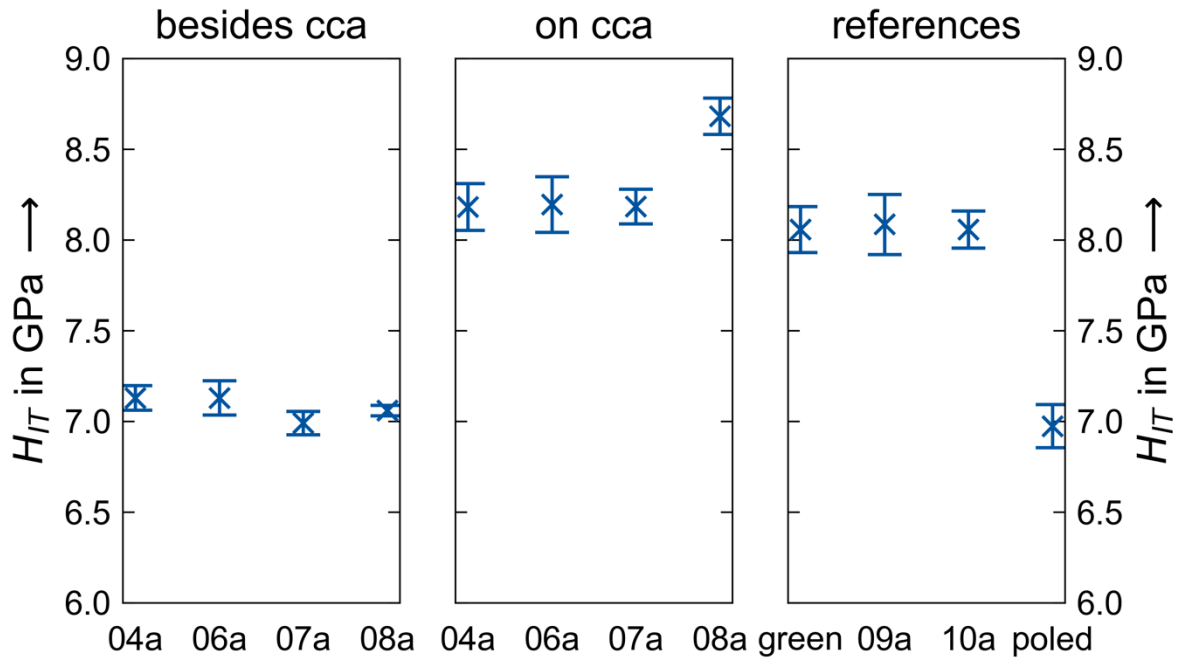

***Figure 9**. Hardness values measured by nanoindentation. The acronym cca stands for crystal contact areas and refers to the Na^+ and K^+ enriched glass regions.*

3.4. XRD

The calculated HQSS mass fractions for sample set b are shown in Figure **10**. For both salt coatings a similar dependency on the poling parameters is visible. A higher poling current as well as a longer poling time decreases the crystal content in the anode side surface of the glass ceramics. This behaviour has been shown and explained before, compare. [21], [33] Looking at samples with the same poling parameters but coated differently (e. g. 9h @ 200 µA, i.e. samples 04b and 08b), a smaller crystal fraction of HQSS can be found in the KCl coated compared to the NaCl coated samples, but still more than in an uncoated and poled sample. This effect is most likely the cause of two things. Firstly, the salt coatings shield the glass underneath from the electric field to a certain degree due to the dielectric behaviour of these salts. Therefore, the Li^+ depletion effect is not as strong for the coated samples as for the uncoated samples which results in a higher crystallinity in the glass-ceramic surface. Secondly, the difference in crystal content between NaCl and KCl coated samples could be due to the different rate of diffusion of Na^+ and K^+. Whereas Na^+ spreads fast during the ceramisation heating, K^+ is more stationary and therefore stays mostly in the surface layer. During crystallisation K^+ disturbs the diffusion-controlled crystal growth as Li^+ needs to diffuse to the crystal and K^+ needs to diffuse away for the HQSS to form. Hence, the K^+ accumulation in the surface could lead to a retardation of crystallisation and a slightly lower crystal content than in the NaCl coated samples.

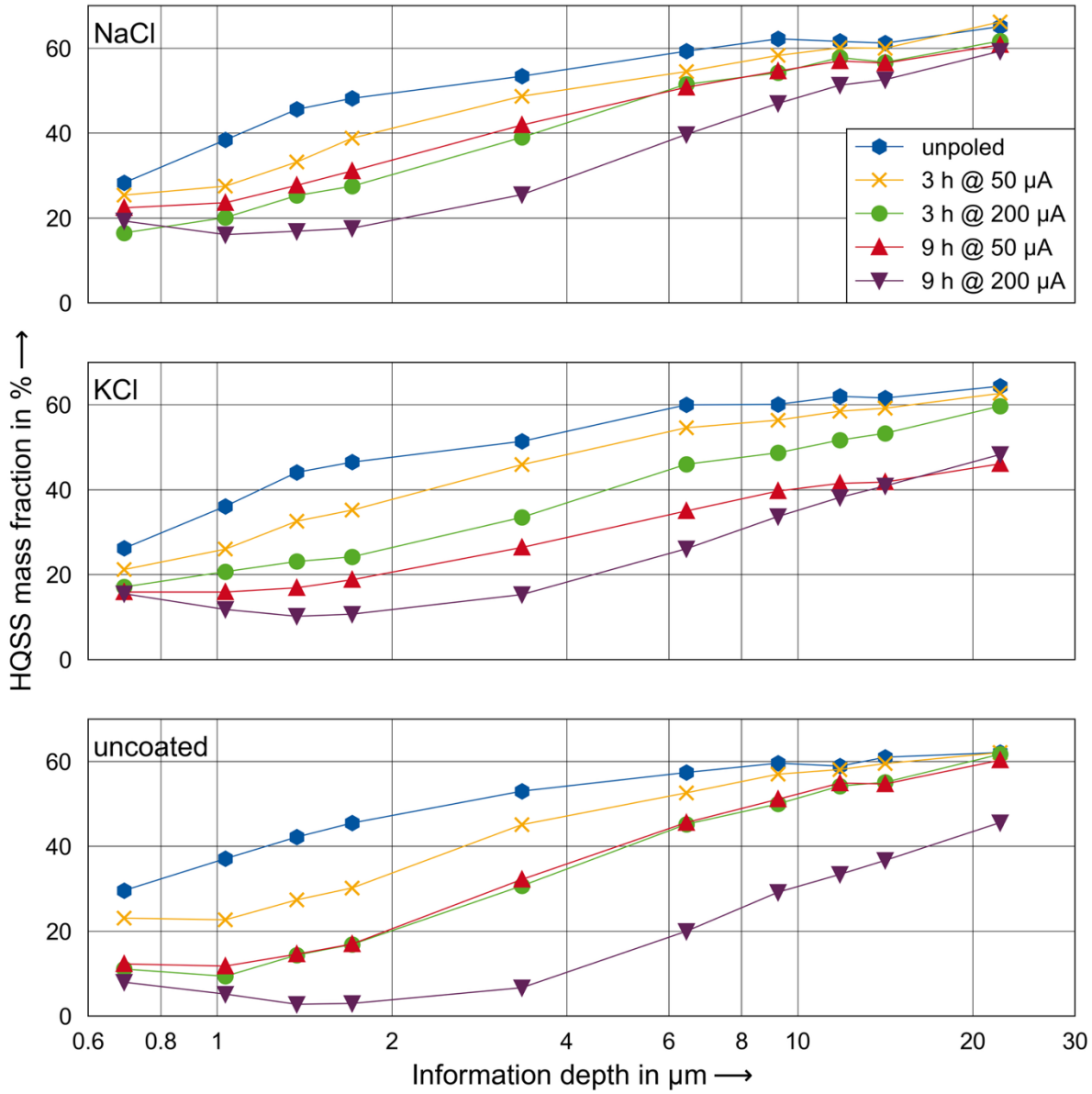

***Figure 10**. HQSS mass fractions in the anode side sample surfaces. The error was around one percent which is smaller than the marker sizes and therefore it is not shown in the graph.*

3.5. Chemical Durability

The etching depths measured with WLI showed no dependency regarding the thermal poling parameters and the different salt coatings. This suggests that the electric field strength and the duration of thermal poling treatment only influences the depletion layer thickness but not the structural changes itself as proposed by Sander. [34] However, differences between the crystal contact areas and the non-coated areas appeared.

Figure **11** shows an example of the surface topology of the etched areas of samples 04a and 08a. The previously protruded crystal contact areas have changed to craters of 300 nm to 400 nm depth. This indicates a faster etching rate of the Na^+ and K^+ enriched glass areas, which coincides with studies regarding the composition dependent etching rates in silicate glasses. These studies show faster etching for (earth-) alkali metal containing glasses due to a weakened silicate network or in other words less Si-O-Si bonds that have to be broken during dissolution because of the presence of more NBOs. [35]

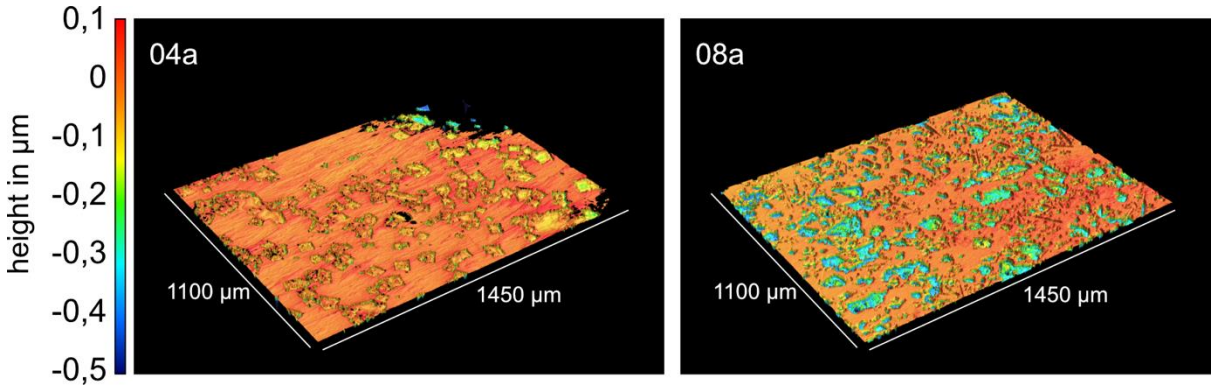

***Figure 11**. Surface topologies of 04a and 08a after etching trials. For better visibility the z-axes are magnified by 5000 %.*

For the glass-ceramic samples, the Na^+ and K^+ enriched surface areas act differently than for the glass samples. After the etching trials the crystal contact areas become more visible and, opposite to the glasses, these areas now protrude from the surrounding surface. In Figure **12** WLI images of the etched surfaces of samples 04b and 08b are shown as well as EDX mappings of etched crystal contact areas. As the EDX measurements show, these regions have a slightly smaller Na^+ or K^+ content than the surrounding glass, which is an inversion to the pre-ceramised condition shown in Figure ***4*** and also the pre-etched glass-ceramics in Figure **7**.

One explanation could be a segregation effect during crystallisation combined with a locally weakened Li depletion due to the salt coating. The salt crystals dampen the electric field and lead to a slightly higher Li^+ content in the cca, so that crystallisation here is preferred. But as the Na^+ and K^+ content in these areas is quite high, these ions are pushed out into the surrounding glass phase during crystallisation as they cannot be incorporated into the HQSS crystal phase. This results in areas with high crystallinity at the cca surrounded by Na^+ or K^+ enriched glass phase. During etching the glass phase is dissolved faster than the crystal phase [36] which leads to the slight protrusion of the crystal contact areas. To bring this into accordance with the pre-etched state, where the salt crystal contact areas still had a Na^+ or K^+ enrichment, one has to look at the information depth of EDX measurements. The interaction volume range R of the electron beam with the analysed material can be calculated using the Kanaya-Okayama equation [37]:

$$R = \frac{2.76 \cdot 10^{-7} \cdot A \cdot E_0^{\frac{5}{3}}}{\rho \cdot Z^{\frac{8}{9}}} \quad (2)$$

With a mean atomic weight A of 24.6 g and a mean atomic number Z of 11.9 (both calculated from the glass composition given in Table **1**), an incident energy E_0 of 15 keV and a measured density ρ of 2.45 g/cm^3 the expected penetration depth of the electrons is around 2.8 µm. Comparing this to the 1-2 µm thick glassy surface layer seen in Figure **6** means that most of the information during EDX surface mappings of the pre-etched glass-ceramics comes from this exact layer. As also seen in Figure **6**, where the precipitated salt crystals were in contact with this glass layer, these locations are enriched in the respective ions (at least for K^+). After etching to about 1 -2 µm depth this glassy top layer is removed, revealing the underlying crystal phase which then was confirmed with EDX mappings again and showed the expected Na^+ and K^+ depletion.

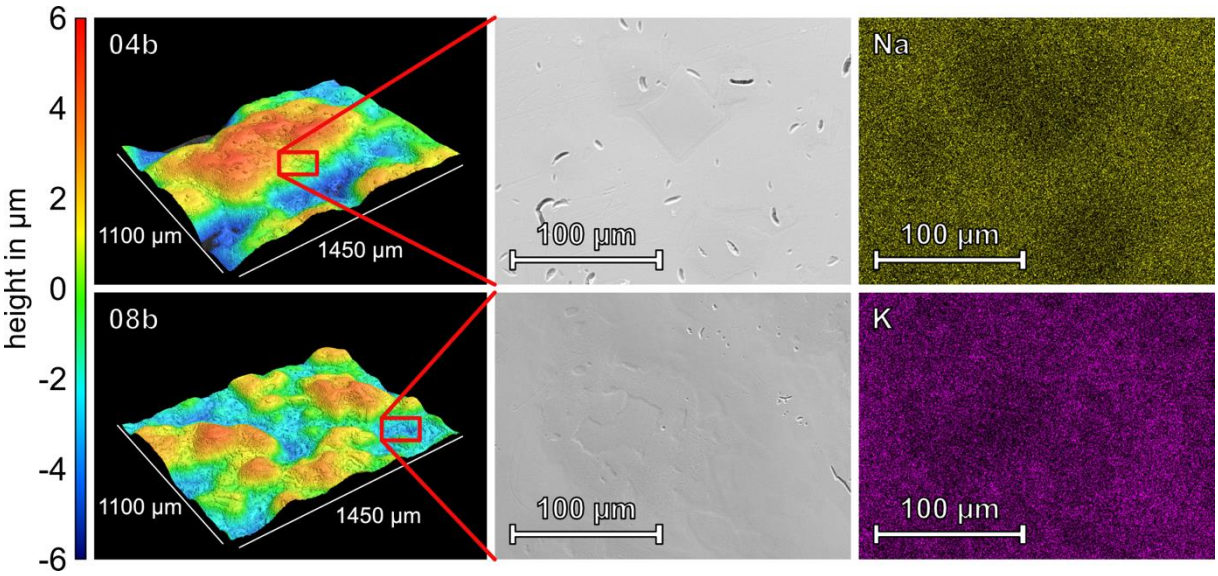

***Figure 12**. Surface topologies and crystal contact areas of 04b and 08b after the etching trials. For better visibility the z-axes are magnified by 1500 %.*

4. Conclusion

A thermal poling setup with an open electrode configuration was used to introduce Na^+ and K^+ cations from chloride salt coatings into the anode side of LAS glass. The cations enter the glass only perpendicular to the glass surface along the electric field lines at the salt crystal contact areas up to 15 µm deep for Na^+ and up to 4 µm deep for K^+. The large cations lead to a measurable volume increase in the glass surface. Compression stresses build up which eventually manifest in a higher surface hardness at the crystal contact areas. The Na^+ and K^+ enriched surface areas etch faster in 5 % HF than the surrounding glass due to the altered chemistry and thus weakened glass structure.

After a heat treatment for ceramisation, the obtained glass-ceramics show a very uneven surface. Presumably, the heterogeneous salt coating and therefore the heterogeneous cation insertion leads to locally different crystallisation behaviour. In combination with changed viscosity this is resulting in a piling up of material at the sample surfaces. At the high temperature (860 °C) needed for ceramisation the sharp concentration profiles of Na^+ and K^+ vanish due to diffusion. For Na^+ only slight concentration differences can be measured whereas K^+ at least partially accumulates in a 1-2 µm thin glassy surface layer of the glass-ceramics. The applied salt coatings lead to a higher crystal content in the first few micrometres of the glass-ceramics compared to uncoated and thermally poled samples. This is most likely the result of electric shielding of the salts during thermal poling and therefore weakening of the Li^+ depletion. After etching trials, the salt crystal contact areas become more visible again as they protrude from the surface which means that they etch away more slowly than the rest of the glass-ceramics. SEM-EDX show a slight depletion of Na^+ and K^+ in these areas which could be a result of segregation during crystallisation and with that explain the altered etching behaviour.

This work has shown that thermal poling can be used to introduce cations from salt coatings into glass surfaces and influence properties such as surface hardness or crystallisation behaviour. By optimising the coating process and investigating other coating compositions it should be possible to create homogeneous surface modifications of glasses and glass-ceramics.

Data availability statement

Data of presented results can be provided upon request.

Author contributions

Jonas Hildebrand: Conceptualisation, Investigation, Data analysis, Visualisation, Writing – original draft. Christian Roos: Conceptualisation, Project administration, Resources, Funding acquisition, Writing – review and editing

Competing interests

The authors declare that they have no competing interests.

Acknowledgement

The authors thank Philipp Jacobs for performing the XRD measurements and Ralf Coenen for operating the SEM.

References

[1] R. J. Charles, 'Polarization and Diffusion in a Silicate Glass', *Journal of Applied Physics*, vol. 32, no. 6, pp. 1115–1126, June 1961, doi: 10.1063/1.1736169.

[2] P. M. Sutton, 'Space Charge and Electrode Polarization in Glass, I', *Journal of the American Ceramic Society*, vol. 47, no. 4, pp. 188–194, Apr. 1964, doi: 10.1111/j.1151-2916.1964.tb14390.x.

[3] D. E. Carlson, K. W. Hang, and G. F. Stockdale, 'Electrode "Polarization" in Alkali-Containing Glasses', *J American Ceramic Society*, vol. 55, no. 7, pp. 337–341, July 1972, doi: 10.1111/j.1151-2916.1972.tb11305.x.

[4] M. Dussauze *et al.*, 'How Does Thermal Poling Affect the Structure of Soda-Lime Glass?', *J. Phys. Chem. C*, vol. 114, no. 29, pp. 12754–12759, July 2010, doi: 10.1021/jp1033905.

[5] M. Chazot *et al.*, 'Enhancement of mechanical properties and chemical durability of Soda-lime silicate glasses treated by DC gas discharges', *J. Am. Ceram. Soc.*, vol. 104, no. 1, pp. 157–166, Jan. 2021, doi: 10.1111/jace.17438.

[6] E. C. Ziemath, V. D. Araújo, and C. A. Escanhoela, 'Compositional and structural changes at the anodic surface of thermally poled soda-lime float glass', *Journal of Applied Physics*, vol. 104, no. 5, p. 054912, Sept. 2008, doi: 10.1063/1.2975996.

[7] M. Dussauze, E. I. Kamitsos, E. Fargin, and V. Rodriguez, 'Refractive index distribution in the non-linear optical layer of thermally poled oxide glasses', *Chemical Physics Letters*, vol. 470, no. 1–3, pp. 63–66, Feb. 2009, doi: 10.1016/j.cplett.2009.01.007.

[8] W. Margulis and F. Laurell, 'Fabrication of waveguides in glasses by a poling procedure', *Applied Physics Letters*, vol. 71, no. 17, pp. 2418–2420, Oct. 1997, doi: 10.1063/1.120079.

[9] A. Canagasabey, C. Corbari, Z. Zhang, P. G. Kazansky, and M. Ibsen, 'Broadly tunable second-harmonic generation in periodically poled silica fibers', *Opt. Lett.*, vol. 32, no. 13, p. 1863, July 2007, doi: 10.1364/OL.32.001863.

[10] P. St. J. Russell, C. N. Pannell, P. G. Kazansky, and L. Dong, 'Pockels effect in thermally poled silica optical fibres', *Electronics Letters*, vol. 31, no. 1, pp. 62–63, Jan. 1995, doi: 10.1049/el:19950036.

[11] J. Luo *et al.*, 'Chemical structure and mechanical properties of soda lime silica glass surfaces treated by thermal poling in inert and reactive ambient gases', *J Am Ceram Soc*, vol. 101, no. 7, pp. 2951–2964, July 2018, doi: 10.1111/jace.15476.

[12] H. He, J. Luo, L. Qian, C. G. Pantano, and S. H. Kim, 'Thermal Poling of Soda-Lime Silica Glass with Nonblocking Electrodes-Part 2: Effects on Mechanical and Mechano-chemical Properties', *J. Am. Ceram. Soc.*, vol. 99, no. 4, pp. 1231–1238, Apr. 2016, doi: 10.1111/jace.14080.
[13] A. Lipovskii, V. Zhurikhina, and D. Tagantsev, '2D-structuring of glasses via thermal poling: A short review', *Int J of Appl Glass Sci*, vol. 9, no. 1, pp. 24–28, Jan. 2018, doi: 10.1111/ijag.12273.
[14] O. Deparis, P. G. Kazansky, A. Abdolvand, A. Podlipensky, G. Seifert, and H. Graener, 'Poling-assisted bleaching of metal-doped nanocomposite glass', *Applied Physics Letters*, vol. 85, no. 6, pp. 872–874, Aug. 2004, doi: 10.1063/1.1779966.
[15] K. M. Knowles and A. T. J. Van Helvoort, 'Anodic bonding', *International Materials Reviews*, vol. 51, no. 5, pp. 273–311, Oct. 2006, doi: 10.1179/174328006X102501.
[16] G. Pintori and V. M. Sglavo, 'Electric-field assisted ion-exchange of innovative float glass', *Journal of Non-Crystalline Solids*, vol. 600, p. 121994, Jan. 2023, doi: 10.1016/j.jnoncrysol.2022.121994.
[17] A. Talimian and V. M. Sglavo, 'Electric Field-Assisted Ion Exchange of Borosilicate Glass Tubes', in *Ion Exchange - Studies and Applications*, A. Kilislioglu, Ed., InTech, 2015. doi: 10.5772/60805.
[18] A. Talimian, G. Mariotto, and V. M. Sglavo, 'Electric field-assisted ion exchange strengthening of borosilicate and soda lime silicate glass', *Int J of Appl Glass Sci*, vol. 8, no. 3, pp. 291–300, Sept. 2017, doi: 10.1111/ijag.12266.
[19] A. Talimian, P. Scardi, and V. M. Sglavo, 'Sodium-caesium electric field assisted ion exchange in a mixed-alkali (Na, K) lime silicate glass', *Journal of Non-Crystalline Solids*, vol. 550, p. 120390, Dec. 2020, doi: 10.1016/j.jnoncrysol.2020.120390.
[20] A. K. Varshneya, G. A. Olson, and P. K. Kreski, 'Strengthended glass and methods for making utilizing electric field assist', US 2015/0166407A1, Dec. 07, 2014
[21] J. Hildebrand and C. Roos, 'Open Electrode Thermal Poling Setup for Treating Lithium-Aluminosilicate Glass-Ceramics Using Gas Discharge', *Glass Eur*, vol. 2, pp. 45–54, Aug. 2024, doi: 10.52825/glass-europe.v2i.1320.
[22] A. Jambon and J.-P. Carron, 'Diffusion of Na, K, Rb and Cs in glasses of albite and orthoclase composition', *Geochimica et Cosmochimica Acta*, vol. 40, no. 8, pp. 897–903, Aug. 1976, doi: 10.1016/0016-7037(76)90138-1.
[23] A. Jambon, 'Tracer diffusion in granitic melts: Experimental results for Na, K, Rb, Cs, Ca, Sr, Ba, Ce, Eu to 1300 °C and a model of calculation', *J. Geophys. Res.*, vol. 87, no. B13, pp. 10797–10810, Dec. 1982, doi: 10.1029/JB087iB13p10797.
[24] G. N. Greaves *et al.*, 'A structural basis for ionic diffusion in oxide glasses', *Philosophical Magazine A*, vol. 64, no. 5, pp. 1059–1072, Nov. 1991, doi: 10.1080/01418619108204878.
[25] G. J. Lauth and J. Kowalczyk, 'Diffusion', in *Einführung in die Physik und Chemie der Grenzflächen und Kolloide*, Berlin, Heidelberg: Springer Berlin Heidelberg, 2016, pp. 143–187. doi: 10.1007/978-3-662-47018-3_6.
[26] X. Wu, J. D. Moskowitz, J. C. Mauro, M. Potuzak, Q. Zheng, and R. Dieckmann, 'Sodium tracer diffusion in sodium boroaluminosilicate glasses', *Journal of Non-Crystalline Solids*, vol. 358, no. 12–13, pp. 1430–1437, July 2012, doi: 10.1016/j.jnoncrysol.2012.03.004.
[27] X. Wu and R. Dieckmann, 'Sodium tracer diffusion in a sodium aluminosilicate glass', *Journal of Non-Crystalline Solids*, vol. 357, no. 22–23, pp. 3797–3802, Nov. 2011, doi: 10.1016/j.jnoncrysol.2011.07.038.
[28] G. H. Frischat, 'Sodium Diffusion in SiO_2 Glass', *J American Ceramic Society*, vol. 51, no. 9, pp. 528–530, Sept. 1968, doi: 10.1111/j.1151-2916.1968.tb15681.x.
[29] S. Karlsson, L. Wondraczek, S. Ali, and B. Jonson, 'Trends in Effective Diffusion Coefficients for Ion-Exchange Strengthening of Soda-Lime-Silicate Glasses', *Front. Mater.*, vol. 4, p. 13, Apr. 2017, doi: 10.3389/fmats.2017.00013.
[30] C. Venkateswaran, H. Sreemoolanadhan, and R. Vaish, 'Lithium aluminosilicate (LAS) glass-ceramics: a review of recent progress', *International Materials Reviews*, vol. 67, no. 6, pp. 620–657, Aug. 2022, doi: 10.1080/09506608.2021.1994108.

[31] J. Luo, H. He, N. J. Podraza, L. Qian, C. G. Pantano, and S. H. Kim, 'Thermal Poling of Soda-Lime Silica Glass with Nonblocking Electrodes-Part 1: Effects of Sodium Ion Migration and Water Ingress on Glass Surface Structure', *J. Am. Ceram. Soc.*, vol. 99, no. 4, pp. 1221–1230, Apr. 2016, doi: 10.1111/jace.14081.
[32] D. R. Tadjiev and R. J. Hand, 'Surface hydration and nanoindentation of silicate glasses', *Journal of Non-Crystalline Solids*, vol. 356, no. 2, pp. 102–108, Jan. 2010, doi: 10.1016/j.jnoncrysol.2009.10.005.
[33] M. Sander, P. Engelmann, P. Jacobs, and C. Roos, 'Controlled surface crystallization of lithium-zinc-alumosilicate glass-ceramics using thermal poling', *J Am Ceram Soc*, vol. 105, no. 5, pp. 3279–3290, May 2022, doi: 10.1111/jace.18301.
[34] M. Sander, 'Structure and properties of thermally poled lithium alumosilicate glasses and glass-ceramics', Dept. of Glass and Glass-Ceramic, RWTH Aachen University, Aachen, Germany, 2023.
[35] G. A. C. M. Spierings, 'Wet chemical etching of silicate glasses in hydrofluoric acid based solutions', *J Mater Sci*, vol. 28, no. 23, pp. 6261–6273, Dec. 1993, doi: 10.1007/BF01352182.
[36] D. Liang and D. W. Readey, 'Dissolution Kinetics of Crystalline and Amorphous Silica in Hydrofluoric-Hydrochloric Acid Mixtures', *Journal of the American Ceramic Society*, vol. 70, no. 8, pp. 570–577, Aug. 1987, doi: 10.1111/j.1151-2916.1987.tb05708.x.
[37] K Kanaya and S Okayama, 'Penetration and energy-loss theory of electrons in solid targets', *J. Phys. D: Appl. Phys.*, vol. 5, no. 1, pp. 43–58, Jan. 1972, doi: 10.1088/0022-3727/5/1/308.